THE JOURNAL OF BIOLOGICAL CHEMISTRY VOL. 290, NO. 22, pp. 13948–13957, May 29, 2015
Published in the U.S.A.

A Point Mutation in the Ubiquitin Ligase RNF170 That Causes Autosomal Dominant Sensory Ataxia Destabilizes the Protein and Impairs Inositol 1,4,5-Trisphosphate Receptor-mediated Ca^{2+} Signaling*

Received for publication, March 26, 2015, and in revised form, April 15, 2015 Published, JBC Papers in Press, April 16, 2015, DOI 10.1074/jbc.M115.655043

Forrest A. Wright[‡], Justine P. Lu[‡], Danielle A. Sliter[§], Nicolas Dupré[¶], Guy A. Rouleau[‖], and Richard J. H. Wojcikiewicz[‡1]

From the [‡]Department of Pharmacology, SUNY Upstate Medical University, Syracuse, New York 13210, the [§]NINDS, National Institutes of Health, Bethesda, Maryland 20892, the [¶]Neuromuscular and Neurogenetic Disease Clinic, CHU de Québec, Laval University, Quebec City, Quebec G1J 1Z4, Canada, and the [‖]Montreal Neurological Institute and Hospital and Department of Neurology and Neurosurgery, McGill University, Montreal, Quebec H3A 2B4, Canada

Background: RNF170 is an endoplasmic reticulum membrane ubiquitin ligase that when mutated at arginine 199 causes a neurodegenerative disease.
Results: The mutation disrupts salt bridges between transmembrane domains, destabilizes the protein, and inhibits Ca^{2+} signaling via IP_3 receptors.
Conclusion: These manifestations of the mutation are likely causative to neurodegeneration.
Significance: Understanding the mechanism of action of mutant ubiquitin ligases will lead to better therapies.

RNF170 is an endoplasmic reticulum membrane ubiquitin ligase that contributes to the ubiquitination of activated inositol 1,4,5-trisphosphate (IP_3) receptors, and also, when point mutated (arginine to cysteine at position 199), causes autosomal dominant sensory ataxia (ADSA), a disease characterized by neurodegeneration in the posterior columns of the spinal cord. Here we demonstrate that this point mutation inhibits RNF170 expression and signaling via IP_3 receptors. Inhibited expression of mutant RNF170 was seen in cells expressing exogenous RNF170 constructs and in ADSA lymphoblasts, and appears to result from enhanced RNF170 autoubiquitination and proteasomal degradation. The basis for these effects was probed via additional point mutations, revealing that ionic interactions between charged residues in the transmembrane domains of RNF170 are required for protein stability. In ADSA lymphoblasts, platelet-activating factor-induced Ca^{2+} mobilization was significantly impaired, whereas neither Ca^{2+} store content, IP_3 receptor levels, nor IP_3 production were altered, indicative of a functional defect at the IP_3 receptor locus, which may be the cause of neurodegeneration. CRISPR/Cas9-mediated genetic deletion of RNF170 showed that RNF170 mediates the addition of all of the ubiquitin conjugates known to become attached to activated IP_3 receptors (monoubiquitin and Lys^{48}- and Lys^{63}-linked ubiquitin chains), and that wild-type and mutant RNF170 have apparently identical ubiquitin ligase activities toward IP_3 receptors. Thus, the Ca^{2+} mobilization defect seen in ADSA lymphoblasts is apparently not due to aberrant IP_3 receptor ubiquitination. Rather, the defect likely reflects abnormal ubiquitination of other substrates, or adaptation to the chronic reduction in RNF170 levels.

In eukaryotic cells, ubiquitin ligases (E3)[2] work together with ubiquitin-conjugating enzymes (E2) to promote ubiquitination of a range of substrates, often leading to their degradation by the proteasome (1–5). Mammals express hundreds of E3s, the vast majority of which contain a RING domain, a motif that appears to provide a docking site for E2s and be necessary for ubiquitin transfer to the substrate (3–5). Endoplasmic reticulum (ER)-associated degradation (ERAD) is the term used to describe the pathway by which aberrant ER lumen or membrane proteins are removed from the cell via ubiquitination and proteasomal degradation (6, 7). A recent bioinformatic survey of RING domain-containing proteins that localize to the ER membrane and that could play a role in ERAD identified a group of 24 E3s (8), some of which (*e.g.* HRD1) appear be capable of mediating the ubiquitination of a broad array of substrates, whereas others (*e.g.* TRC8) have a much narrower substrate range (3, 6, 7). Furthermore, several of the E3s identified (*e.g.* RNF170) have yet to be fully characterized (8).

Inositol 1,4,5-trisphosphate receptors (IP_3Rs) are ER membrane proteins that form tetrameric Ca^{2+} channels that govern ER Ca^{2+} store release (9, 10). When persistently activated, a portion of cellular IP_3Rs are ubiquitinated and degraded by the proteasome apparently via the ERAD pathway, and this IP_3R "down-regulation" suppresses Ca^{2+} mobilization (11, 12).

* This work was supported, in whole or in part, by National Institutes of Health Grant DK049194 and the National Ataxia Foundation.
[1] To whom correspondence should be addressed: 750 E. Adams St., Syracuse, NY 13210. Tel.: 315-464-7956; Fax: 315-464-8014; E-mail: wojcikir@upstate.edu.

[2] The abbreviations used are: E3, ubiquitin ligase; IP_3, inositol 1,4,5-trisphosphate; IP_3R, inositol 1,4,5-trisphosphate receptor; ER, endoplasmic reticulum; ERAD, ER-associated degradation; ADSA, autosomal dominant sensory ataxia; TM, transmembrane; E2, ubiquitin-conjugating enzyme; PAF, platelet-activating factor; GnRH, gonadotropin-releasing hormone; endo H, endoglycosidase H; $[Ca^{2+}]_c$, cytosolic Ca^{2+} concentration.

Recent studies on the mechanism of IP_3R processing by the ERAD pathway have shown that a complex composed of the integral ER membrane proteins erlin1 and erlin2 associates rapidly with activated IP_3Rs (11–14), as does RNF170 (15). RNF170 is ~257 amino acids in length, is highly conserved in mammals, is predicted to have 3 transmembrane (TM) domains, with the RING domain facing the cytosol (15, 16), and is constitutively associated with the erlin1/2 complex. RNF170 contributes to IP_3R ubiquitination (15), although whether it is responsible for the addition of all of the conjugates that become attached to activated IP_3Rs (monoubiquitin and Lys^{48}- and Lys^{63}-linked ubiquitin chains) (17, 18) is currently unknown. Remarkably, a recent molecular genetic study demonstrated that autosomal dominant sensory ataxia (ADSA), a rare neurodegenerative disease characterized by ataxic gait, reduced sensory perception, and neurodegeneration in the posterior columns of the spinal cord, segregates with an arginine (Arg^{199}) to cysteine mutation in human RNF170 (16, 19). Here we examine the effects of this mutation on the properties of RNF170 and find that it destabilizes the protein because of disruption of a salt bridge between TM domains 2 and 3, and that mutant RNF170 disrupts Ca^{2+} signaling at the IP_3R locus in ADSA lymphoblasts. Genetic deletion of RNF170 revealed that RNF170 mediates the addition of all ubiquitin conjugates to activated IP_3Rs and that the ubiquitin ligase activities of wild-type and mutant RNF170 toward activated IP_3Rs are apparently identical. Thus, aberrant ubiquitination of other substrates, or cellular adaptation to chronically reduced RNF170 levels likely accounts for the ADSA-associated Ca^{2+} signaling deficit.

Experimental Procedures

Materials—HeLa cells were cultured as described (13). Human lymphoblast cell lines were isolated from control and affected individuals (16) and cultured in Iscove's modified Dulbecco's medium (Thermo Scientific) supplemented with 10% fetal bovine serum, 50 units/ml of penicillin, 50 μg/ml of streptomycin, and 1 mM L-glutamine. Lymphoblasts were cultured in flasks, fed every 2–3 days, and subcultured 1:10 once per week. Lipofectamine was from Invitrogen, anti-FLAG epitope clone M2 was from Sigma, anti-HA epitope clone HA11 was from Covance, anti-ubiquitin clone FK2 and MG-132 were from BioMol International, anti-RNF170, anti-erlin1, anti-erlin2, anti-Hrd1, anti-gp78, anti-IP_3R1, and anti-IP_3R2 were prepared as described (13–15, 20), anti-β-tubulin was from Cell Signaling Technology, anti-p97 was from Research Diagnostics Inc., anti-p53 clone DO-1 was from Santa Cruz Biotechnology, anti-IP_3R3 was from BD Biosciences, anti-Lys^{48} and anti-Lys^{63} linkage-specific antibodies were a generous gift from Genentech, anti-IP_3R1–3, which recognizes all IP_3R types equally well (21), was a generous gift from Dr. Jan Parys (KU Leuven, Belgium), endoglycosidase H (endo H) was from New England Biolabs, and fura2-AM, cycloheximide, platelet-activating factor (PAF), and gonadotropin-releasing hormone (GnRH) were from Sigma.

Plasmids—Mouse and human RNF170 cDNAs were cloned from mouse αT3 cells and human lymphoblasts as described (15). $RNF170^{FLAG}$ was constructed by ligating the sequence encoding the 257-amino acid mouse RNF170 into the KpnI and BamHI sites of the pCMV14–3xFLAG expression vector such that a triple FLAG tag (DYKDHDGDYKDHDIDYKDDDDKG) is spliced to the C terminus (15). $RNF170^{HA}$ was constructed by PCR amplification of mouse and human RNF170 cDNAs, such that an HA tag (GYPYDVPDYAG) is spliced to the C terminus. Additional constructs were created via PCR that encode proteins with an optimal *N*-glycosylation consensus sequence (NSTMMS) (22) immediately after the HA tag, and with a variety of amino acid substitutions. Primer sequences are available upon request.

Expression and Analysis of RNF170 Constructs—To analyze the expression of exogenous RNF170 and its mutants, HeLa cells (750,000/well of a 6-well plate) were transfected (7 μl of Lipofectamine plus 4.8 μg of total DNA), and 24–48 h later cells were collected with 155 mM NaCl, 10 mM HEPES, 1 mM EDTA, pH 7.4. Cells were then centrifuged (2,300 × *g* for 1 min), disrupted for 30 min at 4 °C with lysis buffer (150 mM NaCl, 50 mM Tris-HCl, 1 mM EDTA, 1% Triton X-100, 10 μM pepstatin, 0.2 mM PMSF, 0.2 μM soybean trypsin inhibitor, 1 mM dithiothreitol, pH 8.0), centrifuged (16,000 × *g* for 10 min at 4 °C), and supernatant samples were subjected to SDS-PAGE and immunoblotting as described (13–15). For studying the interaction between the erlin1/2 complex and RNF170 by co-immunoprecipitation (15), cells were disrupted using lysis buffer that contained 1% CHAPS instead of Triton X-100. The ubiquitin ligase activity of immunopurified $RNF170^{FLAG}$ constructs was assessed as described (15).

Lymphoblasts—To assess protein expression in cell lysates, lymphoblasts were collected by centrifugation (1,000 × *g* for 5 min), washed once by resuspension in PBS followed by centrifugation (16,000 × *g* for 1 min), disrupted for 30 min at 4 °C with 1% CHAPS lysis buffer, centrifuged (16,000 × *g* for 10 min at 4 °C), and supernatant samples were subjected to SDS-PAGE and immunoblotting as described (13–15). For measurement of the cytosolic free Ca^{2+} concentration ($[Ca^{2+}]_c$), lymphoblasts were collected by centrifugation (1,000 × *g* for 1 min), washed once, and then incubated in culture medium at 2 mg of protein/ml with 5 μM fura2-AM for 1 h at 37 °C, washed 4 times with Krebs HEPES buffer (23), and finally resuspended at 0.5 mg of protein/ml in Krebs HEPES buffer for measurement of $[Ca^{2+}]_c$ at 37 °C, as described (23). For measurement of IP_3 levels, lymphoblasts were collected by centrifugation (1,000 × *g* for 5 min), washed once by resuspension in RPMI 1640 (Cellgro) followed by centrifugation (1,000 × *g* for 5 min), resuspended in RPMI 1640 and preincubated at 37 °C for 1 h, then exposed to vehicle (DMSO) or PAF, and IP_3 mass was measured as described (23).

Generation and Analysis of RNF170 Knock-out and Reconstituted Cell Lines—The CRISPR/Cas9 system (24, 25) was used to target an exon within the mouse *RNF170* gene that was common to all predicted splice variants (exon 6). Oligonucleotides that contained the RNF170 target CRISPR sequence (*GATACTGGCGATACGGGTCCTGG*) were annealed and then ligated into AflII-linearized gRNA vector (Addgene). αT3 mouse pituitary cells were transfected (18) with a mixture of the gRNA construct and vectors encoding Cas9 (Addgene) and EGFP (Clontech). Two days post-transfection, EGFP-expressing cells were selected by fluorescence-activated cell sorting

and plated at ~1 cell/well in 96-well plates. Colonies were expanded and screened for ablation of RNF170 expression by immunoblotting with anti-RNF170 (raised against amino acids 50–65 of RNF170) (15). Of the cell lines screened, ~30% lacked RNF170 and 2 of those were expanded for characterization of IP_3R1 processing with essentially identical results; clone IC8 was used for the experiments shown in Fig. 7. Reconstituted cell lines were obtained by transfecting clone IC8 with cDNAs encoding mouse RNF170 and ^{R198C}RNF170 (18), followed by selection in 1.3 mg/ml of G418 for 72 h, plating at ~1 cell/well in 96-well plates, colony expansion, screening with anti-RNF170, and maintenance in 0.3 mg/ml of G418. 2 clones expressing each construct were characterized with essentially identical results.

For analysis of IP_3R1 ubiquitination and protein levels, cells were incubated with 1% CHAPS lysis buffer lacking dithiothreitol, but supplemented with 5 mM *N*-ethylmaleimide, for 30 min at 4 °C, followed by addition of 5 mM dithiothreitol and centrifugation (16,000 × *g* for 10 min at 4 °C). Lysates were then incubated with anti-IP_3R1 to immunoprecipitate IP_3R1 as described (15) and complexes were heated at 37 °C for 30 min prior to SDS-PAGE in 5% gels for ubiquitin conjugate analysis, or 100 °C for 5 min prior to SDS-PAGE in 10% gels for analysis of other proteins. $[Ca^{2+}]_c$ was measured as described (23).

Data Presentation—All experiments were repeated at least once, and representative images of gels or traces are shown. Immunoreactivity was detected and quantitated using Pierce ECL reagents and a GeneGnome Imager (Syngene Bio Imaging). Quantitated data are expressed as mean ± S.E. or range of *n* independent experiments.

Results

Analysis of the Membrane Topology of RNF170—The predicted topology of mouse RNF170, derived from bioinformatic analysis, together with the amino acid sequences of TM domains 2 and 3 are depicted in Fig. 1*A*. The sequence of human RNF170 is very similar to that of mouse RNF170 (91% identical) and human RNF170 has the same predicted topology (15, 16). Note that Arg^{199} in the human sequence corresponds to Arg^{198} in the mouse sequence, because of the absence of Asp^{16} from the latter (15, 16). The existence of TM domains 2 and 3 was confirmed experimentally, using a series of truncation mutants containing a C-terminal HA/glycosylation tag that together with an assessment of sensitivity to the deglycosylating activity of endo H, can provide information on orientation across the ER membrane (22, 26) (Fig. 1*B*). That full-length RNF170 (^{N267}RNF170^{HA}) is insensitive to endo H (and is therefore not glycosylated) localizes the C terminus of this construct to the cytosol (Fig. 1*B*). In contrast, the sensitivity of ^{N230}RNF170^{HA} to endo H shows that the C terminus of this construct is glycosylated and is within the ER lumen, demonstrating that TM2 traverses the ER membrane (Fig. 1*B*). Following the same logic, that ^{N200}RNF170^{HA} is insensitive to endo H and is not glycosylated localizes the C terminus of this construct to the cytosol and confirms the orientation of TM2 (Fig. 1*B*). Finally, to confirm the location of the N terminus, ^{G8N}RNF170^{FLAG} was created, which due to replacement of Gly^8 with asparagine, contains an *N*-glycosylation consensus sequence (NQS) (22, 26) very near the N terminus. This construct was partially glycosylated, indicating that the N terminus is located in the ER lumen (Fig. 1*B*); that the glycosylation was relatively weak may be because the consensus sequence is suboptimal in comparison to the optimal sequence (NSTMMS) present in the other constructs (22). Overall, these data are consistent with the topology of TM domains 1, 2, and 3 shown in Fig. 1*A*.

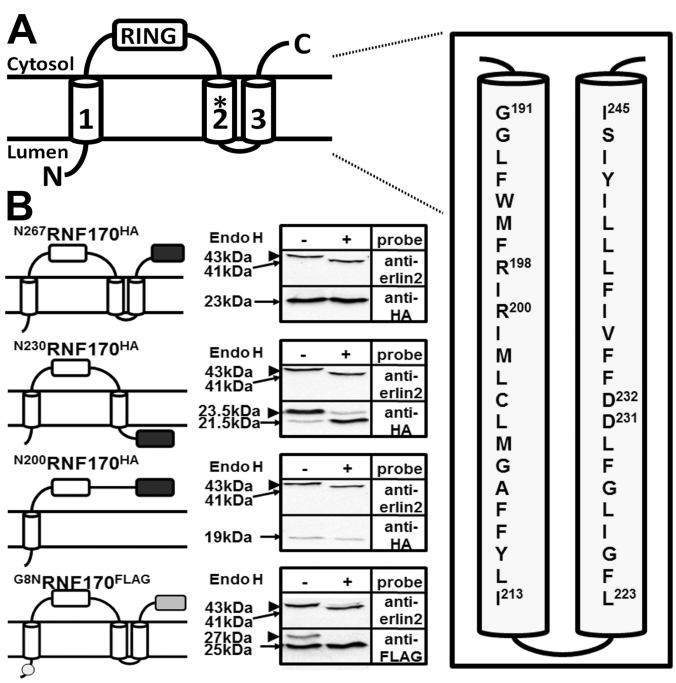

FIGURE 1. **Membrane topology of RNF170.** *A*, predicted topology of RNF170 (15) with the TM2/3 region expanded to show the mouse amino acid sequence. Note that the amino acid that corresponds to Arg^{199} of human RNF170 is Arg^{198} in mouse RNF170, and that the sequences of human and mouse TM2/3 regions are identical, with the exception that Met^{202} of mouse RNF170 is Ile^{203} in human RNF170 (15, 16). The RING domain, the three TM domain regions, and the N and C termini are indicated, and Arg^{198} is identified with an *asterisk*. The precise limits of the predicted TM domains have not been defined experimentally, but the scheme shown is predicted by multiple programs (*e.g.* TMHMM, TOPCONS, etc). *B, N*-glycosylation of RNF170 mutants. An HA/glycosylation tag (*black box*) was introduced at the C terminus of full-length RNF170 (^{N267}RNF170^{HA}), or truncated RNF170 lacking putative TM domain 3 (^{N230}RNF170^{HA}), or putative TM domains 2 and 3 (^{N200}RNF170^{HA}). These, and ^{G8N}RNF170^{FLAG} (FLAG tag indicated by a *gray box* and the G8N mutation with a *circle*) were expressed in HeLa cells, lysates were incubated without or with 1 unit/μl of endo H for 3 h at 37 °C, and samples were subjected to SDS-PAGE. Blots were then probed with anti-HA or anti-FLAG to identify the exogenous RNF170 constructs, or anti-erlin2 to identify endogenous erlin2, which is known to be *N*-glycosylated (13, 14), and which serves as a positive control for endo H. The migration positions of unmodified and *N*-glycosylated species are indicated with *arrows* and *arrowheads*, respectively; degylcosylation of erlin2, ^{N230}RNF170^{HA}, and ^{G8N}RNF170^{FLAG} by endo H reduces their apparent molecular masses by ~2 kDa.

Effects of the Arg^{198} to Cys mutation on RNF170—Remarkably, the Arg^{198} to Cys mutation significantly reduced RNF170 expression. This was seen when the mutation was introduced into either untagged RNF170 or RNF170^{FLAG} (Fig. 2*A*). Furthermore, the mutants migrated ~1 kDa more rapidly than their wild-type counterparts (Fig. 2*A*). Additional mutants were made to explore the basis for the reduction in expression and the migration shift, using RNF170^{FLAG} as a template (Fig. 2*B*). To examine the possibility that these changes resulted from disulfide bond formation with the newly introduced cysteine,

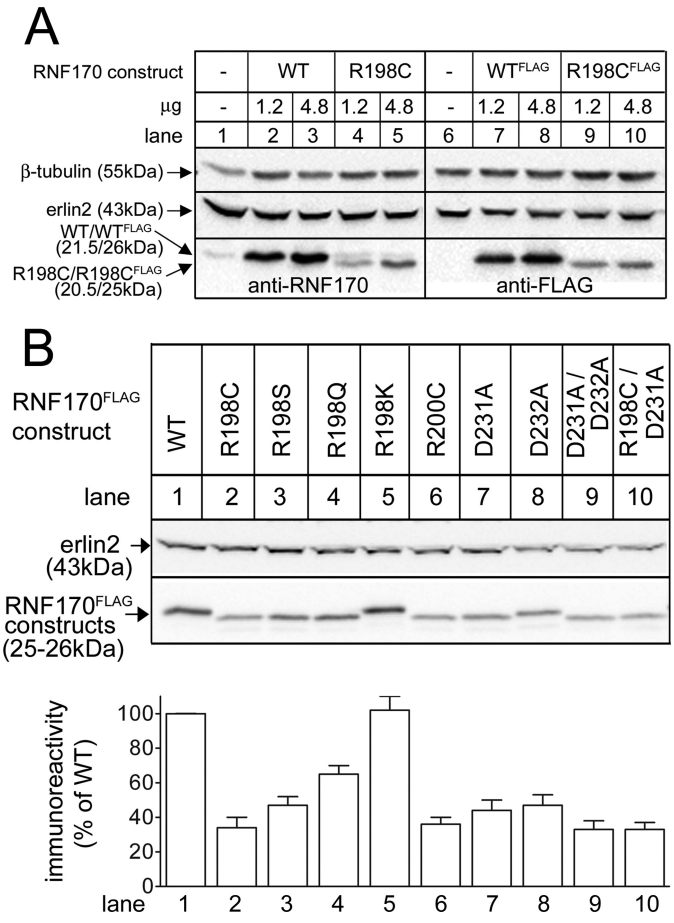

FIGURE 2. **Effects of mutation of Arg^{198} and other amino acids on RNF170 expression.** cDNAs encoding wild-type (WT) and mutant RNF170 constructs and vector alone were transfected into HeLa cells and cell lysates were probed as indicated. Erlin2 and β-tubulin served as loading controls. *A*, lysates were probed with anti-RNF170, which detects both endogenous and exogenous untagged RNF170 constructs (*lanes 1–5*), or with anti-FLAG, which detects just exogenous FLAG-tagged constructs (*lanes 6–10*). *B*, lysates were probed with anti-FLAG and the histogram shows combined quantitated immunoreactivity (mean ± S.E., $n \geq 3$).

Arg^{198} was replaced with serine, which is similar in size to cysteine, but which cannot form disulfide bonds. However, ^{R198S}RNF170^{FLAG} was also expressed poorly and migrated rapidly (Fig. 2*B*, *lane 3*), ruling out a role for disulfide bonds. Likewise, to examine whether the changes were due to loss of the bulky side chain of arginine, or the positive charge, Arg^{198} was replaced with glutamine, which is relatively bulky, but is uncharged, albeit polar. ^{R198Q}RNF170^{FLAG} was also expressed quite poorly and migrated rapidly (*lane 4*), suggesting that it is not the bulk of arginine, but rather its positive charge, that is necessary for normal expression and migration. This was confirmed by replacing Arg^{198} with lysine, which has a slightly shorter side chain, but is still positively charged; ^{R198K}RNF170^{FLAG} was expressed and migrated similarly to ^{WT}RNF170^{FLAG} (*lane 5*).

Examination of the amino acid sequences of TM domains 2 and 3 (Fig. 1*A*) revealed the presence of an additional arginine in TM2 (Arg^{200}) and two aspartic acids in TM3 (Asp^{231} and Asp^{232}) (Fig. 1*A*), suggesting that ionic interactions between TM2 and TM3 could be required for wild-type behavior. Mutation of these amino acids confirmed this notion, as ^{R200C}RNF170^{FLAG}, ^{D231A}RNF170^{FLAG}, ^{D232A}RNF170^{FLAG}, and $^{D231A/D232A}$RNF170^{FLAG} all expressed poorly and migrated more rapidly than RNF170^{FLAG} (*lanes 6–9*). Thus, ionic interactions between arginines in TM2 and aspartic acids in TM3 appear to be required for normal expression of RNF170. Furthermore, it appears that 2 charged amino acids in each TM are required for normal expression, because mutation of one arginine and one aspartic acid in $^{R198C/D231A}$RNF170^{FLAG} did not rescue expression (*lane 10*). Finally, it is noteworthy that accelerated migration correlated well with reduced expression (Fig. 2*B*) and was caused by both arginine and aspartic acid loss and is therefore not due to a change in net protein charge. Rather, these data, together with the fact that RNF170 migrates at 21.5 kDa rather than the predicted 30 kDa (15), suggest that RNF170 is not fully denatured during SDS-PAGE and that the mutations affect the structural organization that is retained. The mutations may also alter the structure of RNF170 *in vivo*, which in turn, could account for the reductions in expression, perhaps because of protein destabilization.

Mechanism of Reduced Expression—To explore possible destabilization mechanisms, we examined the effects of the proteasome inhibitor MG-132. When incubated with cells expressing exogenous RNF170^{FLAG} constructs (Fig. 3*A*), MG-132 caused a marked accumulation of ^{R198C}RNF170^{FLAG} (*lanes 4–6*), although leaving ^{WT}RNF170^{FLAG} levels essentially unaltered (*lanes 1–3*). Thus, the proteasome appears to mediate the reduced expression of ^{R198C}RNF170^{FLAG}. Furthermore, as E3 autoubiquitination is a commonly observed phenomenon (27), we examined the effects of inactivating ligase activity on ^{R198C}RNF170^{FLAG} expression. Previously, we have shown that mutation of Cys^{101} and His^{103} in the RING domain of mouse RNF170 blocks ubiquitin ligase activity (15), and introduction of these mutations into ^{R198C}RNF170^{FLAG} (creating $^{R198C/\Delta RING}$RNF170^{FLAG}) normalized expression (Fig. 3*B*, *lane 4*), suggesting that ligase activity, and most likely autoubiquitination, mediates the reduced expression of ^{R198C}RNF170^{FLAG}. Interestingly, the $^{R198C/\Delta RING}$RNF170^{FLAG} mutant still migrated faster than ^{WT}RNF170^{FLAG}, suggesting that the putative structural change has not been reversed by mutation of the RING domain (Fig. 3*B*, *lane 4*). A role for autoubiquitination was supported by the observation that ^{WT}RNF170^{HA} expression was not differentially affected by co-expression of ^{WT}RNF170^{FLAG} and ^{R198C}RNF170^{FLAG} (Fig. 3*C*, *lanes 2* and 3); this result shows that the apparent destabilizing effect of the R198C mutation is intramolecular and is not transmitted to co-expressed ^{WT}RNF170^{HA} molecules. Importantly, ^{R198C}RNF170^{FLAG} exhibited *in vitro* ubiquitin ligase activity similar to that of ^{WT}RNF170^{FLAG} (Fig. 3*D*, *lanes 2* and *4*), indicating that it is fully capable of autoubiquitinating. Finally, to determine protein half-lives, transfected cells were incubated with the protein synthesis inhibitor cycloheximide (Fig. 3*E*). This revealed that the half-life of ^{R198C}RNF170^{FLAG} is much shorter than that of ^{WT}RNF170^{FLAG}, and that MG-132 blocks ^{R198C}RNF170^{FLAG} degradation. Overall, these data indicate that the R198C mutation decreases RNF170 expression by triggering the molecule to autoubiquitinate and then be degraded by the proteasome.

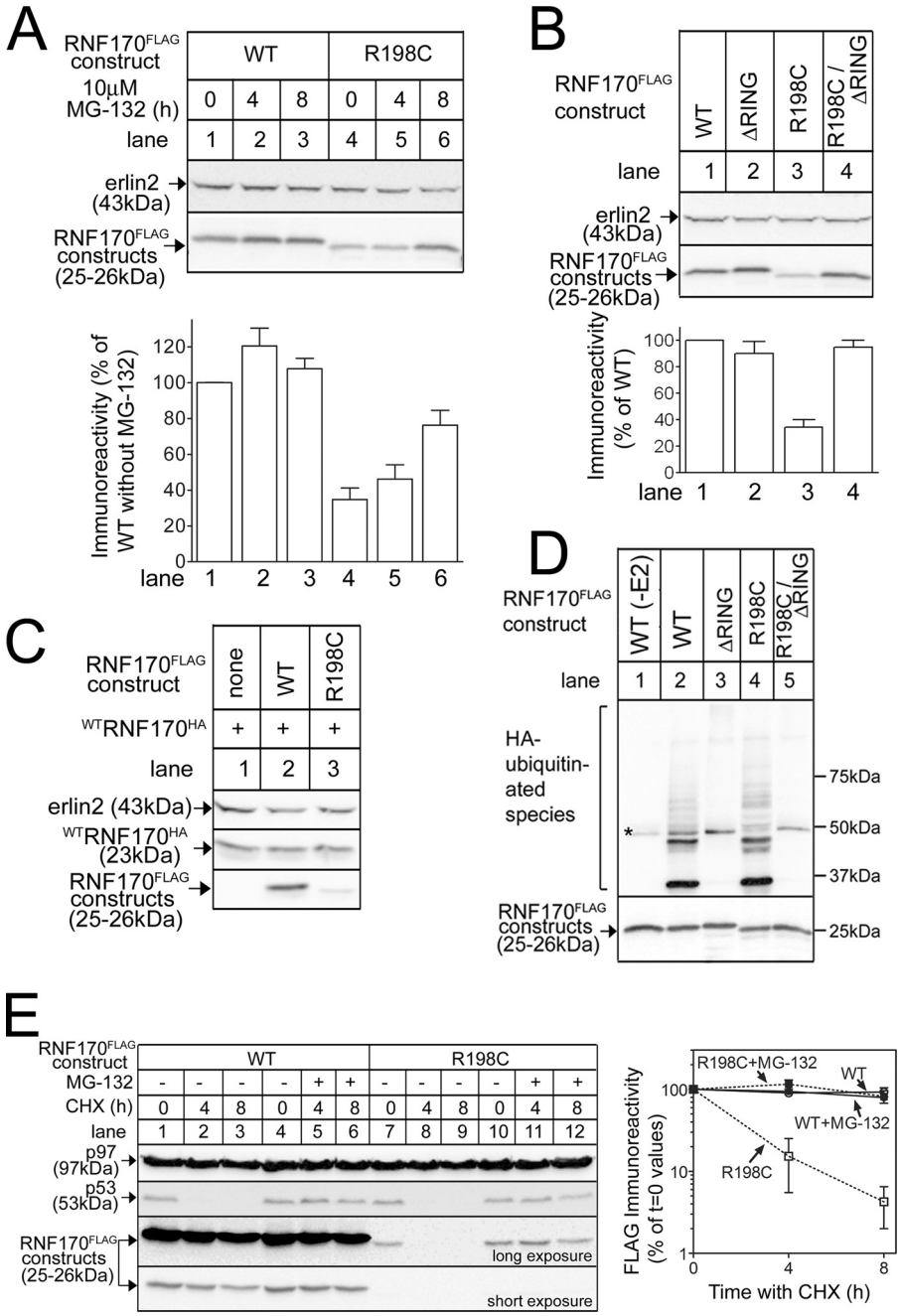

FIGURE 3. **The R198C mutation reduces RNF170 expression via autoubiquitination and the proteasome.** *A-C,* cDNAs encoding tagged WT and mutant RNF170 constructs transfected into HeLa cells were treated as indicated, and cell lysates were probed with anti-FLAG or anti-HA to recognize exogenous RNF170 constructs, or anti-erlin2, which served a loading control. The histograms show combined quantitated immunoreactivity (mean ± S.E., n ≥ 4). *D,* $RNF170^{FLAG}$ constructs were immunopurified from transfected HeLa cells and incubated with E1 (*UBE1*), E2 (*UbcH5b*), and HA-ubiquitin as indicated for 30 min at 30 °C, with the exception of *lane 1*, which lacked E2. Samples were then probed with anti-HA to assess ubiquitination (*upper panel*), or anti-FLAG to assess the levels of $RNF170^{FLAG}$ constructs (*lower panel*). The *asterisk* marks a background band. *E,* transfected HeLa cells were treated as indicated with 20 μg/ml of cycloheximide (*CHX*), without or with 10 μM MG-132. Cell lysates were then probed with anti-p53 as a positive control for cycloheximide action, anti-p97 as a loading control, and anti-FLAG to recognize exogenous RNF170 constructs (long and short exposures are shown to facilitate visualization of immunoreactivity changes). The graph shows combined quantitated FLAG immunoreactivity, using the long exposure for $^{R198C}RNF170^{FLAG}$ and the short exposure for $^{WT}RNF170^{FLAG}$ (mean ± range, $n = 2$).

The R198C Mutation Does Not Alter Membrane Topology, Subcellular Localization, or Interaction with the Erlin1/2 Complex—To explore why mutation-induced salt bridge disruption triggers RNF170 autoubiquitination, we first examined whether subcellular localization was altered. However, the extent of *N*-glycosylation seen for the relevant constructs shown in Fig. 1*B* ($^{N267}RNF170^{HA}$ and $^{N230}RNF170^{HA}$) was not substantially altered by introduction of the R198C mutation (Fig. 4*A*), indicating that localization to the ER and insertion of TM domains is normal. Likewise, interaction with the endogenous erlin1/2 complex was normal, because immunoprecipitation with anti-erlin2 (15) recovered $^{WT}RNF170^{HA}$ and $^{R198C}RNF170^{HA}$ equally well (Fig. 4*B*). Furthermore, membrane association was normal, as both $^{WT}RNF170^{HA}$ and

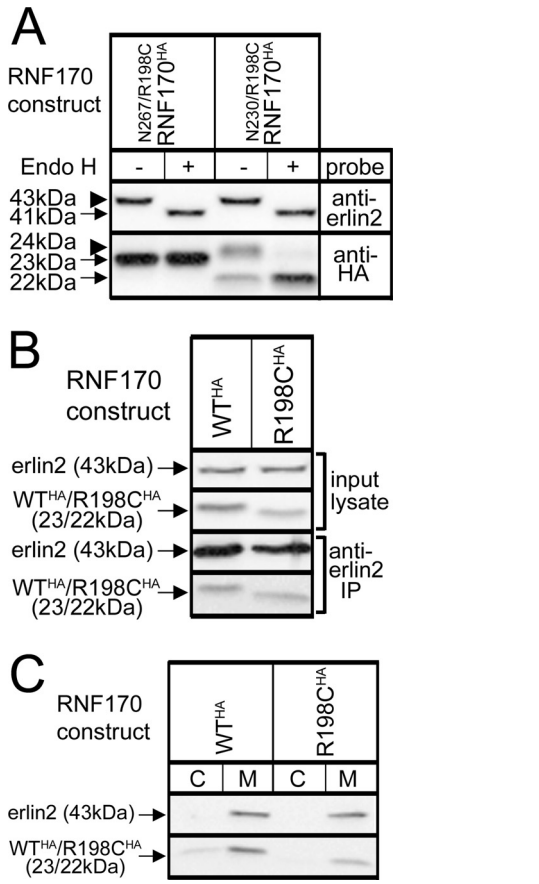

FIGURE 4. **Lack of effect of the R198C mutation on RNF170 membrane association and topology, and interaction with the erlin1/2 complex.** cDNAs encoding HA-tagged WT and mutant RNF170 constructs were transfected into HeLa cells. *A, N*-glycosylation of $^{N267/R198C}$RNF170^{HA} and $^{N230/R198C}$RNF170^{HA}, R198C-containing versions of the constructs shown in Fig. 1*B*, was assessed as described in the legend to Fig. 1*B*. *B,* interaction with the erlin1/2 complex. Erlin1/2 complex was immunoprecipitated with anti-erlin2 was probed for RNF170 constructs (*lower panels*). Note that the amounts of ^{WT}RNF170^{HA} and ^{R198C}RNF170^{HA} that co-immunoprecipitate are proportional to the amounts in input lysates, indicating that they interact with the erlin1/2 complex equally well. *C,* cells were lysed and centrifuged into cytosol (*C*) and membrane (*M*) factions as described (13), and probed as indicated.

^{R198C}RNF170^{HA} were fractionated with membranes (Fig. 4*C*). Thus, the R198C mutation does not dramatically alter the localization of RNF170, indicating that a subtle change in its properties (*e.g.* in the way that it folds) accounts for its apparent autoubiquitination and proteasomal degradation.

RNF170 Expression in Control and ADSA-affected Individuals—Lymphoblast lines from control and ADSA-affected individuals were examined for RNF170 expression (Fig. 5*A*). In controls, an anti-RNF170 immunoreactive band at ~21.5 kDa was observed (*lanes 1–3*), the same size as endogenous HeLa cell RNF170 and untagged mouse RNF170 (Fig. 2*A*). Remarkably, in affected lymphoblasts the strength of the 21.5-kDa band was reduced and an additional weaker band at ~20.5 kDa was also observed (*lanes 4–6*). These results are consistent with the expression level and migration differences seen between exogenous mouse ^{WT}RNF170 and ^{R198C}RNF170 (Fig. 2*A*) and between exogenous human ^{WT}RNF170 and ^{R199C}RNF170 (Fig. 5*B*), and with the knowledge that affected individuals are heterozygote (16). Thus, it appears that the ^{R199C}RNF170 encoded by the mutant allele in affected individuals migrates at ~20.5 kDa and is relatively poorly expressed. This leads to an ~27% reduction in total RNF170 immunoreactivity in affected lymphoblasts (Fig. 5*A*).

Ca^{2+} Mobilization via IP_3 Receptors Is Impaired in Affected Lymphoblasts—Because IP_3Rs are the only known substrates for RNF170 (15), we examined whether IP_3R function was different in control and affected lymphoblasts, using PAF to trigger IP_3R-mediated Ca^{2+} mobilization (28) (Fig. 6). Remarkably, PAF-induced increases in $[Ca^{2+}]_c$ were significantly suppressed in affected lymphoblasts (Fig. 6*A*), suggesting that IP_3R-mediated Ca^{2+} mobilization might be impaired, although the suppression could also be due to an effect on Ca^{2+} entry (29). To rule out any role for Ca^{2+} entry, EGTA was added immediately prior to PAF to chelate extracellular Ca^{2+} to ~100 nM (23), and under these conditions the suppression of PAF-induced increases in $[Ca^{2+}]_c$ was still clearly evident (Fig. 6*B*). To examine if the suppression results from ER Ca^{2+} stores being smaller, cells were exposed to the sarcoplasmic reticulum Ca^{2+}-APTase pump inhibitor thapsigargin, which allows Ca^{2+} leak from the ER in an IP_3R-independent manner (30). However, thapsigargin caused the same $[Ca^{2+}]_c$ increase in control and affected lymphoblasts (Fig. 6*C*), indicating that Ca^{2+} stores are of equal size. Likewise, reduced IP_3 formation was not the reason for the suppression, as PAF-induced increases in IP_3 mass were the same in control and affected lymphoblasts (increases over basal resulting from 0.5 min exposure to 100 nM PAF were 24 ± 8 and 35 ± 15%, respectively; $n = 3$). Finally, measurement of the levels of IP_3R1–3 did not reveal any consistent differences between control and affected lymphoblasts (Fig. 6*D*). Overall, these data indicate that Ca^{2+} mobilization via IP_3Rs is impaired in affected lymphoblasts, but not because of a change in Ca^{2+} store size, or the abundance of IP_3Rs, and point toward a mechanism that involves a regulation of IP_3R activity.

Ubiquitin Ligase Activity of RNF170 and ^{R198C}RNF170 in Cells—^{R198C}RNF170 exhibits apparently normal ubiquitin ligase activity *in vitro* when mixed with purified enzymes (Fig. 3*D*), but that tells us almost nothing about how its activity might differ from that of ^{WT}RNF170 *in vivo*, where the intracellular milieu contains a full complement of E2s, substrates, and other factors. To date, endogenous activated IP_3Rs are the only known substrates for RNF170 (15), but it has yet to be resolved whether RNF170 is responsible for the addition of all of the ubiquitin conjugates that become attached to activated IP_3Rs, or just some (17, 18). Initially, we sought to compare the ligase activities of ^{WT}RNF170 and ^{R199C}RNF170 toward IP_3Rs in control and ADSA lymphoblasts, but pilot experiments showed that to be unfeasible, primarily because of the paucity of IP_3Rs therein (data not shown). Thus, we employed αT3 cells, the cells in which we first identified RNF170 (15) and that exhibit very robust IP_3R1 ubiquitination in response to the IP_3 generating cell surface receptor agonist GnRH (17, 18). First, to determine which ubiquitin conjugates RNF170 adds, we deleted RNF170 using CRISPR/Cas9-mediated gene editing (Fig. 7). RNF170 "knock-out" was specific (Fig. 7*A*), as other pertinent proteins (*e.g.* the ERAD pathway proteins p97, Hrd1, and gp78 (6, 7) and erlins 1 and 2) were expressed at the same level in control and "αT3 RNF170KO" cells. Interestingly, IP_3R1 expression was enhanced ~65% by RNF170 deletion (Fig.

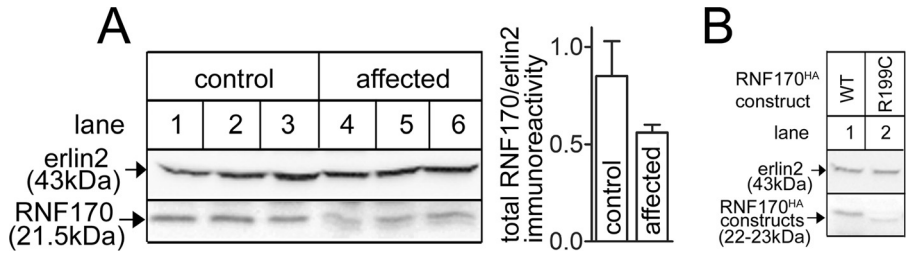

FIGURE 5. **RNF170 levels in lymphoblasts from control and ADSA-affected individuals.** *A*, lysates from 3 control (*lanes 1–3*) and 3 affected individuals (*lanes 4–6*) were probed with anti-RNF170 and anti-erlin2. For the panels shown, immunoreactivity was quantitated and is plotted as total RNF170/erlin2 immunoreactivity (arbitrary units). Multiple quantitations of total RNF170 immunoreactivity from these and other lymphoblast lines showed that affected individuals contained 73 ± 5% of the immunoreactivity seen in control lymphoblasts (n ≥ 5). *B*, cDNAs encoding human ^{WT}RNF170^{HA} and ^{R199C}RNF170^{HA} were transfected into HeLa cells and cell lysates were probed as indicated. Erlin2 served as a loading control.

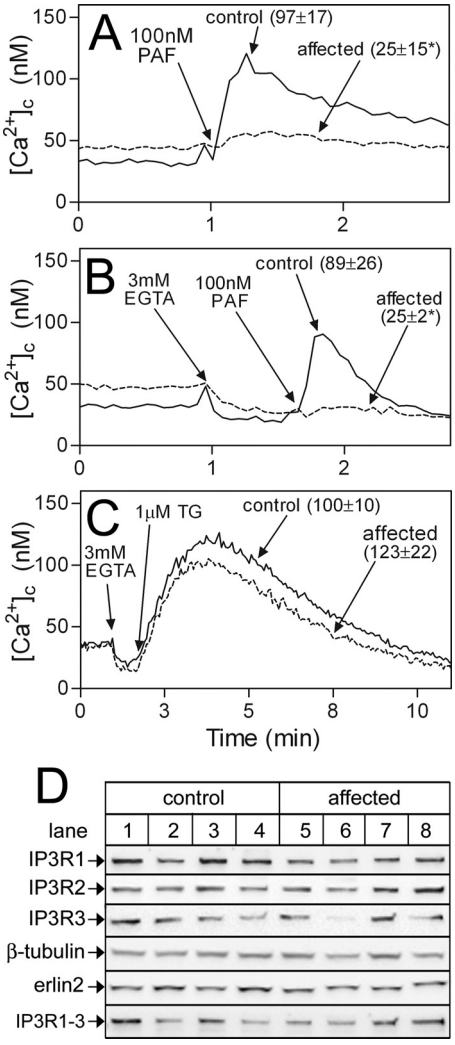

FIGURE 6. **Assessment of the IP_3-medited Ca^{2+} signaling pathway in lymphoblasts.** Multiple control and affected lymphoblast cell lines (*n*) were analyzed. *A–C,* fura2-loaded cells were exposed to PAF, EGTA, and thapsigargin (*TG*) as indicated and $[Ca^{2+}]_c$ was calculated. *Values in parentheses* are mean ± S.E. of PAF- or TG-induced increases in $[Ca^{2+}]_c$ over basal values ($n \geq 4$, with * indicating $p < 0.05$ when comparing values from control *versus* affected cells). *D,* lysates from 4 control and 4 affected lymphoblast lines were probed for the proteins indicated. Total IP_3R immunoreactivity in control and affected lymphoblasts, measured with anti-IP_3R1–3 (*lowest panel*), was 80 ± 20 and 76 ± 15 arbitrary units, respectively (mean ± S.E.).

7, *A* and *D*), indicating that in addition to its role in mediating the degradation of activated IP_3Rs (15), RNF170 also plays a role in basal IP_3R1 turnover. Ca^{2+} mobilization in αT3 RNF170KO cells in response to GnRH was normal (Fig. 7*B*), indicating that the IP_3-dependent signaling pathway and IP_3R activation are not perturbed by the absence of RNF170. Remarkably, deletion of RNF170 completely blocks GnRH-induced IP_3R1 ubiquitination (Fig. 7*C*), observed using either FK2 antibody, which detects all ubiquitin conjugates (monoubiquitin, and Lys^{48}- and Lys^{63}-linked chains), or antibodies specific for Lys^{48}- and Lys^{63}-linked chains (18). In contrast, erlin2 association with IP_3R1 was not blocked, indicating that association of the erlin1/2 complex with activated IP_3R1 is unimpaired, consistent with the notion that it is the erlin1/2 complex that recruits RNF170 to activated IP_3R1, rather than vice versa (12, 15). Thus, RNF170 does indeed catalyze the formation of all ubiquitin conjugates on activated IP_3R1, and as would be expected, GnRH did not cause IP_3R down-regulation in αT3 RNF170KO cells (Fig. 7*D*).

To directly assess the ligase activity of ^{R198C}RNF170, we sought to reconstitute IP_3R ubiquitination in αT3 RNF170KO cells by stably expressing exogenous RNF170 constructs (Fig. 7*E*). Cell lines were obtained, although exogenous expression was less than that seen for endogenous RNF170 in control αT3 cells (data not shown). Both ^{WT}RNF170 and ^{R198C}RNF170 were capable of ubiquitinating activated IP_3Rs, as indicated by increases in Lys^{48}- and Lys^{63}-linked ubiquitin chains and total ubiquitin after exposure to GnRH (Fig. 7*E*). That less ubiquitination was seen in ^{R198C}RNF170-expressing cells is most likely a consequence of lower expression level and IP_3R binding of the mutant (Fig. 7*E*). Thus, the ligase activity of ^{R198C}RNF170 toward IP_3Rs receptors *in vivo* appears to be qualitatively normal, and aberrant IP_3R receptor ubiquitination is unlikely to account for the Ca^{2+} signaling deficit seen in ADSA lymphoblasts.

Discussion

Our data show that the Arg^{198} to Cys mutation in mouse RNF170 reduces the stability and expression level of the protein. The mutation appears to disrupt a salt bridge between TM domains 2 and 3 and leads to autoubiquitination and enhanced turnover via the ubiquitin-proteasome pathway. This mechanism also likely applies to human ^{R199C}RNF170 in ADSA-affected individuals, and accounts for the ~27% reduction in the total cellular complement of RNF170. An equivalent decrease in cellular ligase activity attributable to RNF170 is likely, which could be critical to development of the disease. Alternatively, the ligase activity of mutant RNF170 *in vivo* could be abnormal.

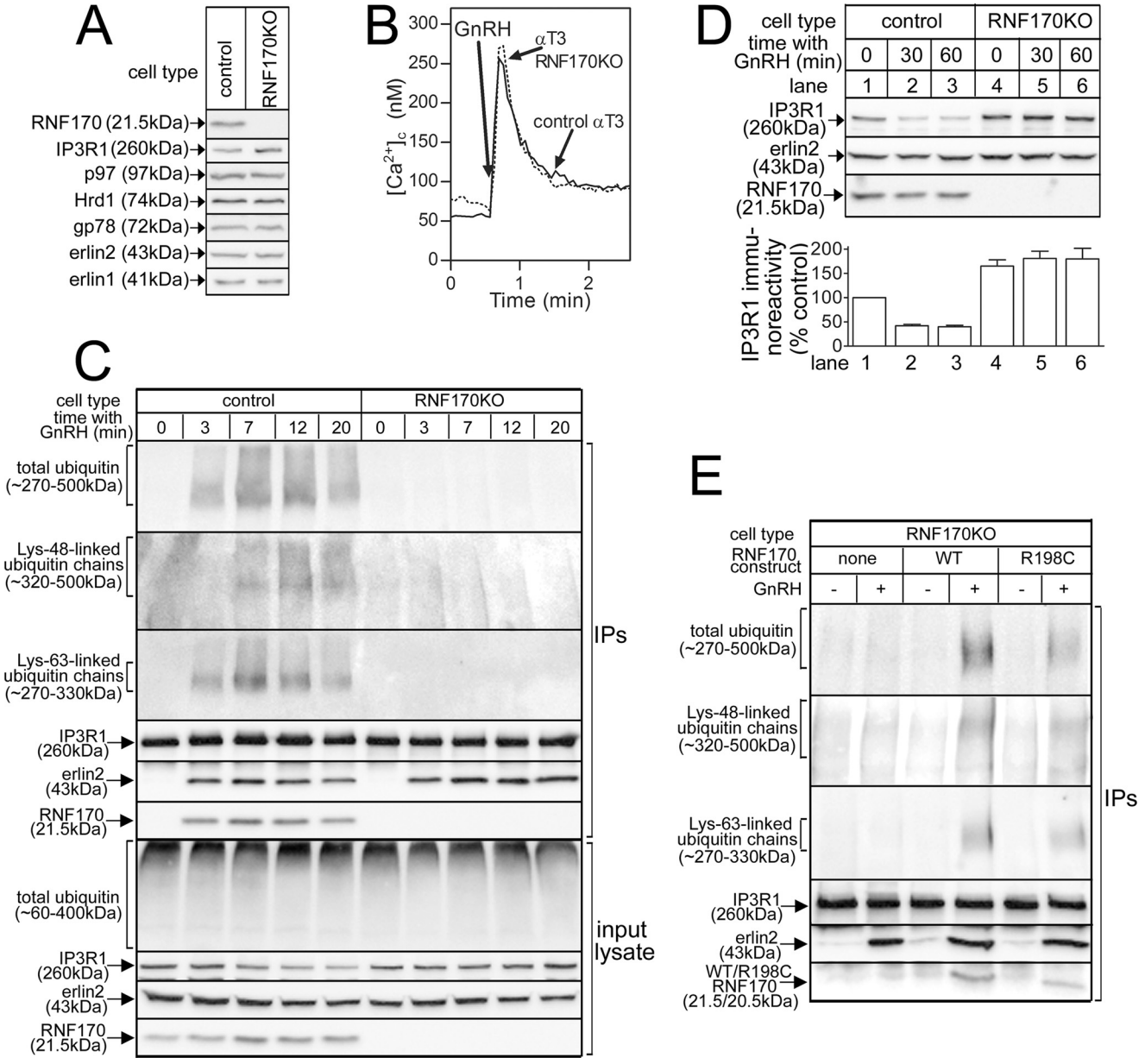

FIGURE 7. **CRISPR/Cas9-mediated deletion of RNF170 and reconstitution with exogenous RNF170 constructs.** *A*, levels of RNF170, IP_3R1, and other pertinent proteins in lysates from αT3 control and RNF170KO cells. *B*, GnRH (0.1 μM)-induced Ca^{2+} mobilization in αT3 control and RNF170KO cells. *C*, IP_3R1 ubiquitination in αT3 control and RNF170KO cells. Cells were incubated with 0.1 μM GnRH and anti-IP_3R1 IPs and input lysates were probed for the proteins indicated. *D*, IP_3R1 down-regulation in αT3 control and RNF170KO cells. Cells were incubated with 0.1 μM GnRH and lysates were probed for the proteins indicated. The histogram shows combined quantitated immunoreactivity (mean ± S.E., $n = 4$). *E*, reconstitution of IP_3R1 ubiquitination in RNF170KO cells. αT3 RNF170KO cells stably expressing ^{WT}RNF170 or ^{R198C}RNF170 were incubated without or with 0.1 μM GnRH for 20 min, and anti-IP_3R1 IPs were probed for the proteins indicated.

We did not obtain support for this notion from studies with purified components *in vitro* (Fig. 3*D*), or from analysis of IP_3R1 ubiquitination *in vivo* (Fig. 7*E*), but that does not rule out the possibility that mutant RNF170 acts abnormally toward other substrates. Mutant RNF170 acting in this manner (*i.e.* dominantly) would be consistent with zebrafish studies, in which expression of exogenous mutant RNF170 causes aberrant development (16).

Prior to the current study, our approach to defining the function of RNF170 (and other proteins suspected to play a role in IP_3R ERAD) has been to deplete them using RNA interference. Although we have had some success with this approach (13–15, 31) it has major limitations; in particular, proteins are only *depleted* and the effects of residual proteins are hard to assess and complicate interpretation of data from reconstitution experiments, and cells expressing short interfering RNA are often unhealthy and are available only in limited quantities. Use of the CRISPR/Cas9 system (24, 25) allowed us to *delete* RNF170 and demonstrate, for the first time, that RNF170 catalyzes the addition of all ubiquitin conjugates to activated IP_3R1. Intriguingly, this suggests that RNF170 interacts with multiple E2s, most likely Ubc13 and Ubc7, because Ubc13 is the only E2 known to build Lys^{63}-linked chains (5, 32) and Ubc7, which builds Lys^{48}-linked

chains (5, 32), is already strongly implicated in mediating IP_3R1 ubiquitination and degradation (33).

Why does the Arg^{198} to Cys mutation destabilize RNF170? It appears that a network of salt bridges couple TM domains 2 and 3 together, because mutation of either Arg^{198} or Arg^{200} in TM2 reduces protein expression, as do mutations to Asp^{231} and Asp^{232} in TM3. A hint as to why these mutations are apparently destabilizing is provided by the fact that they also cause RNF170 to migrate more rapidly on SDS-PAGE, indicative of a structural change in the protein that either causes more compact folding and/or alters interactions with SDS. The structural change appears to be subtle, as the Arg^{198} to Cys mutation did not significantly affect TM2 and TM3 insertion into the ER membrane, or interaction with the erlin1/2 complex, but could still be sufficient to trigger autoubiquitination and targeting for ERAD. Interestingly, many other E3s are known to be regulated by ubiquitination (3, 27), including the ER membrane ligase gp78 (27), which is relatively unstable and is controlled both by autoubiquitination and an additional ER membrane ubiquitin ligase Hrd1 (27). It will be interesting to see whether mutations in the TM domains of gp78 and other ER membrane ligases (8) are also destabilizing.

Although the presence of charged residues in TM domains is energetically unfavorable, such residues are often found therein, where they play important functions, often involving salt bridges (34). Intriguingly, TM domain-located charged residues are those most likely to cause disease when mutated, arginine has the highest propensity for disease causation, and the Arg to Cys mutation is relatively common because cytosine to thymine transition occurs with relatively high frequency (35). Situations very similar to that described here for RNF170 are seen in other proteins. For example, the pore architecture of cystic fibrosis transmembrane conductance regulator is maintained by salt bridges between arginines in TM6 (Arg^{347} and Arg^{352}) and aspartic acids in adjacent TMs (36), and naturally occurring, charge altering mutations of Arg^{352} cause cystic fibrosis (37). Likewise, the naturally occurring R279C mutation in the prostacyclin receptor dramatically reduces protein expression (38).

Remarkably, the expression of ^{R199C}RNF170 correlated with a reduction in PAF-induced Ca^{2+} mobilization in lymphoblasts that was not due to a change in IP_3R levels, but rather appears to result from reduced signal transduction efficiency at the IP_3R locus. This was apparently not due to aberrant IP_3R ubiquitination, as the ubiquitination of activated IP_3R1 in cells expressing wild-type or mutant RNF170 was qualitatively identical, at least in terms of the addition of total ubiquitin and Lys^{48}- and Lys^{63}-linked chains. Rather, the reduction in signal transduction efficiency at the IP_3R locus could be an indirect effect, if RNF170 turns out to ubiquitinate additional substrates (*e.g.* proteins that regulate IP_3Rs), or if long-term adaptation to the ~27% reduction in total RNF170 expression seen in ADSA lymphoblasts alters the expression of genes that govern Ca^{2+} signaling.

Dysregulation of Ca^{2+} metabolism and IP_3R function is often mooted to be the cause of the neurodegeneration that underpins certain spinocerebellar ataxias and neurodegenerative diseases (39–43) and our data suggest that the same could be true for ADSA. If so, therapies aimed at boosting Ca^{2+} mobilization could be contemplated, similarly to the way that manipulating Ca^{2+} metabolism is being examined as a therapy for Huntington disease and other spinocerebellar ataxias (41–43). Interestingly, mutations to erlin2 also cause neurodegenerative diseases (44–47). Erlin2 is the dominant partner in the erlin1/2 complex, to which RNF170 is constitutively associated (11, 12, 15), and the erlin1/2 complex mediates the interaction of RNF170 with IP_3Rs (15). Clearly, defining the mechanisms by which mutations to the erlin1/2 complex-RNF170 axis cause neurodegeneration will be fascinating topics for future study.

Acknowledgments—We thank Erik Vandermark and Jacqualyn Schulman for helpful suggestions.

References

1. Finley, D. (2009) Recognition and processing of ubiquitin-protein conjugates by the proteasome. *Annu. Rev. Biochem.* **78,** 477–513
2. Kleiger, G., and Mayor, T. (2014) Perilous journey: a tour of the ubiquitin-proteasome system. *Trends Cell Biol.* **24,** 352–359
3. Deshaies, R. J., and Joazeiro, C. A. (2009) RING Domain E3 ubiquitin ligases. *Annu. Rev. Biochem.* **78,** 399–434
4. Budhidarmo, R., Nakatani, Y., and Day, C. L. (2012) RINGs hold the key to ubiquitin transfer. *Trends Biochem. Sci.* **37,** 58–65
5. Metzger, M. B., Pruneda, J. N., Klevit, R. E., and Weissman, A. M. (2014) RING-type E3 ligases: master manipulators of E2 ubiquitin-conjugating enzymes and ubiquitination. *Biochim. Biophys. Acta* **1843,** 47–60
6. Ruggiano, A., Foresti, O., and Carvalho, P. (2014) ER-associated degradation: protein quality control and beyond. *J. Cell Biol.* **204,** 869–879
7. Christianson, J. C., and Ye, Y. (2014) Cleaning up in the endoplasmic reticulum: ubiquitin in charge. *Nat. Struct. Mol. Biol.* **21,** 325–335
8. Neutzner, A., Neutzner, M., Benischke, A. S., Ryu, S. W., Frank, S., Youle, R. J., and Karbowski, M. (2011) A systematic search for endoplasmic reticulum (ER) membrane-associated RING finger proteins identifies Nixin/ZNRF4 as a regulator of calnexin stability and ER homeostasis. *J. Biol. Chem.* **286,** 8633–8643
9. Foskett, J. K., White, C., Cheung, K. H., and Mak, D. O. (2007) Inositol trisphosphate receptor Ca^{2+} release channels. *Physiol. Rev.* **87,** 593–658
10. Seo, M. D., Velamakanni, S., Ishiyama, N., Stathopulos, P. B., Rossi, A. M., Khan, S. A., Dale, P., Li, C., Ames, J. B., Ikura, M., and Taylor, C. W. (2012) Structural and functional conservation of key domains in $InsP_3$ and ryanodine receptors. *Nature* **483,** 108–112
11. Wojcikiewicz, R. J., Pearce, M. M., Sliter, D. A., and Wang, Y. (2009) When worlds collide: IP_3 receptors and the ERAD pathway. *Cell Calcium* **46,** 147–153
12. Wojcikiewicz, R. J. (2012) Inositol 1,4,5-trisphosphate receptor degradation pathways. *WIREs Membr. Transp. Signal.* **1,** 126–135
13. Pearce, M. M., Wang, Y., Kelley, G. G., and Wojcikiewicz, R. J. (2007) SPFH2 mediates the endoplasmic reticulum-associated degradation of inositol 1,4,5-trisphosphate receptors and other substrates in mammalian cells. *J. Biol. Chem.* **282,** 20104–20115
14. Pearce, M. M., Wormer, D. B., Wilkens, S., and Wojcikiewicz, R. J. (2009) An endoplasmic reticulum (ER) membrane complex composed of SPFH1 and SPFH2 mediates the ER-associated degradation of inositol 1,4,5-trisphosphate receptors. *J. Biol. Chem.* **284,** 10433–10445
15. Lu, J. P., Wang, Y., Sliter, D. A., Pearce, M. M., and Wojcikiewicz, R. J. (2011) RNF170, an endoplasmic reticulum membrane ubiquitin ligase, mediates inositol 1,4,5-trisphosphate receptor ubiquitination and degradation. *J. Biol. Chem.* **286,** 24426–24433
16. Valdmanis, P. N., Dupré, N., Lachance, M., Stochmanski, S. J., Belzil, V. V., Dion, P. A., Thiffault, I., Brais, B., Weston, L., Saint-Amant, L., Samuels, M. E., and Rouleau, G. A. (2011) A mutation in the RNF170 gene causes autosomal dominant sensory ataxia. *Brain* **134,** 602–607
17. Sliter, D. A., Kubota, K., Kirkpatrick, D. S., Alzayady, K. J., Gygi, S. P., and Wojcikiewicz, R. J. (2008) Mass spectral analysis of type I inositol 1,4,5-trisphosphate receptor ubiquitination. *J. Biol. Chem.* **283,** 35319–35328
18. Sliter D. A., Aguiar, M., Gygi, S. P., and Wojcikiewicz, R. J. (2011) Activated inositol 1,4,5-trisphosphate receptors are modified by homogene-

ous Lys-48- and Lys-63-linked ubiquitin chains, but only Lys-48-linked chains are required for degradation. *J. Biol. Chem.* **286,** 1074–1082
19. Moeller, J. J., Macaulay, R. J., Valdmanis, P. N., Weston, L. E., Rouleau, G. A., and Dupré, N. (2008) Autosomal dominant sensory ataxia: a neuroaxonal dystrophy. *Acta Neuropathol.* **116,** 331–336
20. Wojcikiewicz, R. J. (1995) Type I, II and III inositol 1,4,5-trisphosphate receptors are unequally susceptible to down-regulation and are expressed in markedly different proportions in different cell types. *J. Biol. Chem.* **270,** 11678–11683
21. Bultynck, G., Szlufcik, K., Kasri, N. N., Assefa, Z., Callewaert, G., Missiaen, L., Parys, J. B., and De Smedt, H. (2004) Thimerosal stimulates Ca^{2+} flux through inositol 1,4,5-trisphosphate receptor type 1, but not type 3, via modulation of an isoform-specific Ca^{2+}-dependent intramolecular interaction. *Biochem. J.* **381,** 87–96
22. Bañó-Polo, M., Baldin, F., Tamborero, S., Marti-Renom, M. A., and Mingarro, I. (2011) *N*-glycosylation efficiency is determined by the distance to the C-terminus and the amino acid preceding an Asn-Ser-Thr sequon. *Protein Sci.* **20,** 179–186
23. Wojcikiewicz, R. J., Tobin, A. B., and Nahorski, S. R. (1994) Muscarinic receptor-mediated inositol 1,4,5-trisphosphate formation in SH-SY5Y neuroblastoma cells is regulated acutely by cytosolic Ca^{2+} and by rapid desensitization. *J. Neurochem.* **63,** 177–185
24. Mali, P., Yang, L., Esvelt, K. M., Aach, J., Guell, M., DiCarlo, J. E., Norville, J. E., and Church, G. M. (2013) RNA-guided human genome engineering via Cas9. *Science* **339,** 823–826
25. Ran, F. A., Hsu, P. D., Wright, J., Agarwala, V., Scott, D. A., and Zhang, F. (2013) Genome engineering using the CRISPR-Cas9 system. *Nat. Protoc.* **8,** 2281–2308
26. van Geest, M., and Lolkema, J. S. (2000) Membrane topology and insertion of membrane proteins: search for topogenic signals. *Microbiol. Mol. Biol. Rev.* **64,** 13–33
27. Weissman, A. M., Shabek, N., and Ciechanover, A. (2011) The predator becomes the prey: regulating the ubiquitin system by ubiquitylation and degradation. *Nat. Rev. Mol. Cell Biol.* **12,** 605–620
28. Pietruck, F., Spleiter, S., Daul, A., Philipp, T., Derwahl, M., Schatz, H., and Siffert, W. (1998) Enhanced G protein activation in IDDM patients with diabetic nephropathy. *Diabetologica* **41,** 94–100
29. Rosskopf, D., Daelman, W., Busch, S., Schurks, M., Hartung, K., Kribben, A., Michel, M. C., and Siffert, W. (1998) Growth factor-like action of lysophosphatidic acid on human B lymphoblasts. *Am. J. Physiol.* **274,** C1573–1582
30. Thastrup, O., Cullen, P. J., Drøbak, B. K., Hanley, M. R., and Dawson, A. P. (1990) Thapsigargin, a tumour promoter, discharges intracellular Ca2+ stores by specific inhibition of the endoplasmic reticulum Ca^{2+}-ATPase. *Proc. Natl. Acad. Sci. U.S.A.* **87,** 2466–2470
31. Alzayady, K. J., Panning, M. M., Kelley, G. G., and Wojcikiewicz, R. J. (2005) Involvement of the p97-Ufd1-Npl4 complex in the regulated endoplasmic reticulum-associated degradation of inositol 1,4,5-trisphosphate receptors. *J. Biol. Chem.* **280,** 34530–34537
32. Ye, Y., and Rape, M. (2009) Building ubiquitin chains: E2 enzymes at work. *Nat. Rev. Mol. Cell Biol.* **10,** 755–764
33. Webster, J. M., Tiwari, S., Weissman, A. M., and Wojcikiewicz, R. J. (2003) Inositol 1,4,5-trisphosphate receptor ubiquitination is mediated by mammalian Ubc7, a component of the endoplasmic reticulum-associated degradation pathway, and is inhibited by chelation of intracellular Zn^{2+}. *J. Biol. Chem.* **278,** 38238–38246
34. von Heijne, G. (2006) Membrane-protein topology. *Nat. Rev. Mol. Cell Biol.* **7,** 909–918
35. Partridge, A. W., Therien, A. G., and Deber, C. M. (2004) Missense mutations in transmembrane domains of proteins: phenotypic propensity of polar residues for human disease. *Proteins* **54,** 648–656
36. Cui, G., Freeman, C. S., Knotts, T., Prince, C. Z., Kuang, C., and McCarty, N. A. (2013) Two salt bridges differentially contribute to the maintenance of cystic fibrosis conductance regulator (CFTR) channel function. *J. Biol. Chem.* **288,** 20758–20767
37. Cui, G., Zhang, Z-R., O'Brien, A. R., Song, B., and McCarty, N. A. (2008) Mutations at arginine 352 alter the pore architecture of CFTR. *J. Membr. Biol.* **222,** 91–106
38. Stitham, J., Arehart, E., Gleim, S. R., Li, N., Douville, K., and Hwa, J. (2007) New insights into human prostacyclin receptor structure and function through natural and synthetic mutations of transmembrane charged residues. *Br. J. Pharmacol.* **152,** 513–522
39. Paulson, H. L. (2009) The spinocerebellar ataxias. *J. Neuroopthamol.* **29,** 227–237
40. Matilla-Dueñas, A., Corral-Juan, M., Volpini, V., and Sanchez, I. (2012) The spinocerebellar ataxias: clinical aspects and molecular genetics. *Adv. Exp. Med. Biol.* **724,** 351–374
41. Bezprozvanny, I. (2011) Role of inositol 1,4,5-trisphosphate receptors in pathogenesis of Huntington's disease and spinocerebellar ataxias. *Neurochem. Res.* **36,** 1186–1197
42. Foskett, J. K. (2010) Inositol trisphosphate receptor Ca^{2+} release channels in neurological diseases. *Pfugers Arch*. **460,** 481–494
43. Brown, S. A., and Loew, L. M. (2014) Integration of modeling with experimental and clinical findings synthesizes and refines the central role of inositol 1,4,5-trisphosphate receptor 1 in spinocerebellar ataxia. *Front. Neurosci.* **8,** 453
44. Yildirim, Y., Orhan, E. K., Iseri, S. A., Serdaroglu-Oflazer, P., Kara, B., Solakoğlu, S., and Tolun, A. (2011) A frameshift mutation of erlin2 in recessive intellectual disability, motor dysfunction and multiple joint contractures. *Hum. Mol. Genet.* **20,** 1886–1892
45. Alazami, A. M., Adly, N., Al Dhalaan, H., and Alkuraya, F. S. (2011) A nullimorphiic *erlin2* mutation defines a complicated hereditary spastic paraplegia locus (SPG18). *Neurogenetics* **12,** 333–336
46. Al-Saif, A., Bohlega, S., and Al-Mohanna, F. (2012) Loss of erlin2 function leads to juvenile primary lateral sclerosis. *Ann. Neurol.* **72,** 510–516
47. Wakil, S. M., Bohlega, S., Hagos, S., Baz, B., Al Dossari, H., Ramzan, K., and Al-Hassnan, Z. N. (2013) A novel splice site mutation in erlin2 causes hereditary spastic paraplegia in a Saudi family. *Eur. J. Med. Genet.* **56,** 43–45